Title: Cannabinoid Combination Targets *NOTCH1*-Mutated T-ALL Through the Integrated Stress Response Pathway

Authors

Elazar Besser[1], Anat Gelfand[1], Shiri Procaccia[1], Paula Berman[1], David Meiri[1, *]

Affiliations

[1] The Laboratory of Cancer Biology and Cannabinoid Research, Faculty of Biology, Technion-Israel Institute of Technology, Haifa 3200003, Israel

* Corresponding author: David Meiri, The Laboratory of Cancer Biology and Cannabinoid Research, Faculty of Biology, Technion- Israel Institute of Technology, Haifa 3200003, Israel; Phone: +972-77-8871681; Fax: +972-4-8225153; E-mail: dmeiri@technion.ac.il

15 **Abstract**

16 In T-cell acute lymphoblastic leukemia (T-ALL) more than 50% of cases display autoactivation of Notch1
17 signaling, leading to oncogenic transformation. We have previously identified a specific chemovar of
18 Cannabis that induces apoptosis by preventing Notch1 maturation in leukemia cells. Here, we isolated
19 three cannabinoids from this chemovar that synergistically mimic the effects of the whole extract. Two
20 were previously known, Cannabidiol (CBD) and Cannabidivarin (CBDV); whereas the third cannabinoid,
21 which we termed 331-18A, was identified and fully characterized in this study. We demonstrated that
22 these cannabinoids act through Cannabinoid receptor type 2 and TRPV1 to activate the integrated stress
23 response pathway by depleting intracellular Ca^{2+}. This is followed by increased mRNA and protein
24 expression of ATF4, CHOP and CHAC1, which is hindered by inhibiting the upstream initiation factor
25 eIF2α. The increased abundance of CHAC1 prevents Notch1 maturation, thereby reducing the levels of
26 the active Notch1 intracellular domain, and consequently decreasing cell viability and increasing
27 apoptosis. Treatment with the three isolated molecules resulted in reduced tumor size and weight in-vivo
28 and slowed leukemia progression in mice models. Altogether, this study elucidated the mechanism of
29 action of three distinct cannabinoids in modulating the Notch1 pathway, and constitutes an important step
30 in the establishment of a new therapy for treating *NOTCH1*-mutated diseases and cancers such as T-ALL.

Introduction

T-cell acute lymphoblastic leukemia (T-ALL) is an aggressive cancer, characterized by immature T-lymphoblasts (*1*, *2*). In over 50% of cases, activating mutations in *NOTCH1* were identified, generating much interest in targeting the Notch1 signaling pathway in this disease (*3–5*). The Notch1 protein is a single-pass transmembrane receptor that is expressed on the plasma membrane. It regulates evolutionarily conserved signaling that controls developmental processes, cell fate determination and tissue homeostasis. It is a member of the Notch receptor family, which consists of four receptors (Notch1-4) in humans (*4*, *6*). The Notch1 receptor-signaling pathway is activated through a series of proteolytic cleavages at three different sites (S1–S3). S1 cleavage is carried out by a Furin-like convertase in the trans-Golgi apparatus, resulting in a heterodimeric receptor that is transported to the membrane where it can bind ligands from a neighboring cell. Upon binding of a ligand, cleavage is performed at the next site and the activation of the Notch1 receptor-signaling pathway is initiated, enabling the cleavage of S3 in the transmembrane region that causes the release of the Notch1 intracellular domain (NICD), which translocates to the nucleus where it promotes transcription of target genes involved in cell growth (*7*).

Aberrant Notch1 activity is associated with many other leukemia types and other cancers, including prostate, lung, ovarian, and renal (*8–12*). A new and promising emerging field in cancer treatment is medical Cannabis and its unique active compounds, the phytocannabinoids. Phytocannabinoids affect the body by means of the endocannabinoid system (eCBS), a ubiquitous neuromodulatory signaling system that has widespread functions throughout the body. Notable eCBS receptors include cannabinoid receptor type 1 (CB1) and CB2, which belong to the family of G protein-coupled receptors, and transient receptor potential vanilloid type 1 (TRPV1), which is an ion channel (*13*). The eCBS participates in many physiological activities, including the regulation of Ca^{2+} homeostasis (*14–16*).

Medical Cannabis is already commonly used by cancer patients for its palliative effects, it was shown to stimulate appetite while alleviating symptoms such as nausea, vomiting and pain (*17*). However,

55 accumulating evidence demonstrated phytocannabinoids directly affect tumor development in cell lines
56 and animal models by modulating key cell-signaling pathways (*18–20*). Studies demonstrated that purified
57 phytocannabinoids can inhibit proliferation, metastasis, and angiogenesis and exert pro-apoptotic effects
58 in a variety of cancer cell types such as lung, breast, prostate, skin, intestine, glioma, lymphoma, pancreas
59 and uterine cancers (*21–23*). In preclinical models, treatment with phytocannabinoids led to tumor
60 regression of different cancer types (*24*, *25*).
61 Concerning T-ALL, some studies using phytocannabinoids and their respective formulations (such as
62 Dronabinol) have shown anti-proliferative as well as proapoptotic effects in selected leukemia cell lines
63 and native leukemia blasts cultured *ex-vivo* (*26–28*). Nevertheless, the mechanisms of phytocannabinoid-
64 mediated antitumor effects are not yet fully understood. Most of the studies that examined the anti-cancer
65 effects of Cannabis have focused mainly on the two major phytocannabinoids (−)-*trans*-Δ^9-
66 tetrahydrocannabinol (Δ^9-THC) and Cannabidiol (CBD), but these are just two of more than 140 different
67 phytocannabinoids that have been identified in different Cannabis chemovars (*29*, *30*).
68 We have previously demonstrated that different Cannabis extracts with unique phytocannabinoid
69 compositions impaired the survival and proliferation of specific cancer cell lines, suggesting that the effect
70 of a particular Cannabis extract on a specific cancer cell line relies on its chemical composition (*31*).
71 Following this framework, we successfully matched a specific CBD-rich Cannabis extract to T-ALL
72 leukemia cells that harbor a *NOTCH1* mutation (*32*). In the present study, we investigated which specific
73 metabolites in the whole extract are responsible for T-ALL elimination, and elucidated the molecular
74 mechanism by which they mediate their antitumor effects in this type of cancer.

75 **Results**

76 We have previously shown a specific CBD-rich Cannabis extract selectively induces apoptosis in T-ALL
77 leukemia cell lines that harbor a *NOTCH1* mutation. Treatment led to accumulation of the full-length
78 immature form of Notch1 in the membrane, correspondingly with reduced NICD protein expression and
79 transcription activity (*32*).

80 **A combination of three phytocannabinoids induces apoptosis and reduces NICD expression**

81 The CBD-rich extract was more potent than pure CBD or other high-CBD chemovars (*32*). This implied
82 a specific combination of metabolites from the plant potentiate the full antitumor effect. Using a semi-
83 preparative HPLC, we separated the whole extract into four 10-minute retention time fractions (**Fig. 1A**).
84 A full list of the phytocannabinoids constituting each fraction is presented in supplementary table S1.
85 We assessed the effect of each fraction on the viability of MOLT-4 cells (fig. S1A) and found fraction 2
86 reduced viability to a similar extent as the whole extract. Further analysis revealed that out of the four
87 fractions, only fraction 2 induced apoptotic cell death (Fig. 1B), reduced the protein levels of the NICD
88 (Fig. 1C, D) and elevated the levels of cleaved caspase-3 (Fig. 1D). Thus, we excluded all the
89 phytocannabinoids present in the other three fractions, such as Δ^9-THC in fraction 3.

90 To pinpoint the active phytocannabinoids in fraction 2, we further separated this fraction into individual
91 phytocannabinoids using centrifugal partition chromatography (CPC) followed by semi-preparative
92 HPLC (C1-C5 in Fig. 1E). We identified the specific compounds in the isolated peaks (Supplementary
93 table S2), C2 was identified as cannabidivarin (CBDV) and C5 as CBD. C3 and C4 were identified as
94 Cannabidiolic acid (CBDA), the precursor to CBD, and as CBD-C4, respectively; but their
95 concentrations were very low. C1 was identified as 331-18A, a phytocannabinoid first identified by our
96 team in decarboxylated CBD-rich Cannabis chemovars (*29*), we characterized 331-18A using ESI-
97 LC/MS/MS as having a deprotonated m/z of 331.2279 and MS/MS fragments resembling those of CBD

98 with the addition of one hydroxyl group. To confirm the identification, the purity of the three isolated
99 compounds was determined by UHPLC/UV (fig. S2A-C).

100 Here, we further elucidated the chemical structure of 331-18A by nuclear magnetic resonance (NMR)
101 with CBD as the reference (Supplementary Fig. S3 and table S3). The NMR data of CBD was in close
102 agreement with the literature (*33*). The spectra of CBD and 331-18A were very similar with the exception
103 of the disappearance of the external double bond (C_8-C_{10}) and the appearance of a tertiary alcohol instead.
104 The absolute stereochemistry of 331-18A was confirmed by specific rotation determination with a
105 polarimeter in which 331-18A showed $[\alpha]^{20}_D$ −56.85 which is comparable with the $[\alpha]^{20}_D$ −64.16 of both
106 the CBD that was isolated from the fraction (C5) and a commercial standard of CBD. These results
107 suggested that similarly to CBD, the two substituents at positions 1 and 6 of the cyclohexene ring are in
108 a *trans* configuration (Fig. 1F).

109 To examine the cytotoxic properties of the isolated compounds and their combinations on MOLT-4 cells,
110 the isolated phytocannabinoids were prepared in the same amounts and proportion as observed in the
111 whole extract; for example, if 1 μg of the whole extract contained 50% CBD, we used 0.5 μg of the purified
112 CBD and 1 μg of the whole extract in the respective treatments. Compared to the whole extract, the
113 phytocannabinoids 331-18A and CBDV alone did not induce apoptosis or had minor effects on the cells,
114 and CBD alone induced only 55% cell death compared to the whole extract (Fig. 1G). When CBD was
115 combined with either 331-18A or CBDV, the percent of apoptotic cells increased to 58% and 61%,
116 respectively. The combination of all three phytocannabinoids led to the greatest cytotoxic effect and only
117 this combination was comparable to the whole extract (88.29% ± 4.31% and 93.85% ± 1.64%,
118 respectively). We further evaluated the effect of the three phytocannabinoids separately or in different
119 combinations on the protein expression of NICD (Fig. 1H-I) and found that all combinations of

phytocannabinoids led to a significant reduction in NICD expression, but only when all the three were combined, NICD levels decreased to the same extent as with the whole extract.

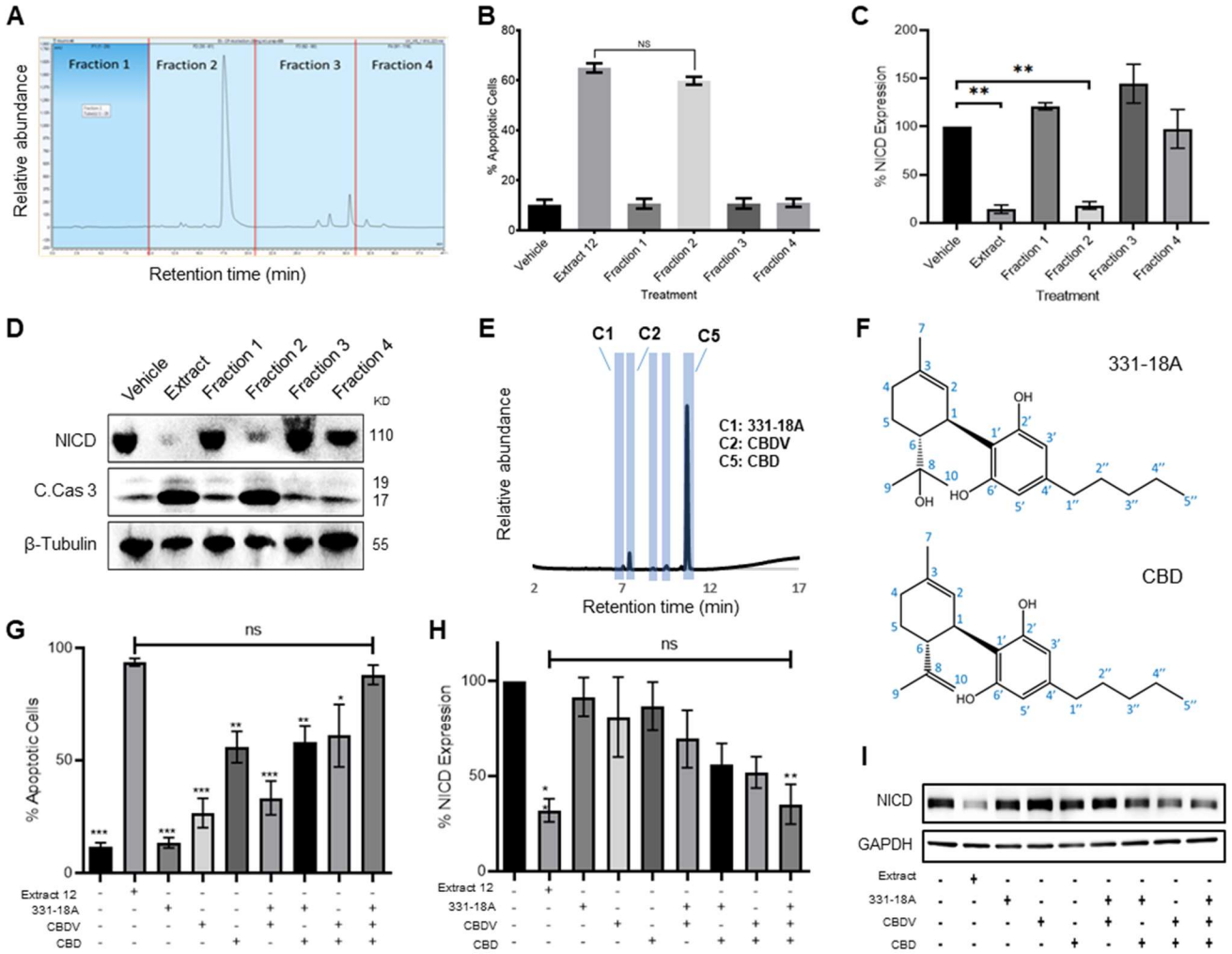

Fig. 1. Identifying specific phytocannabinoids responsible for the cytotoxic effect of the whole extract. (**A**) A semi-preparative HPLC-UV chromatogram of the whole extract showing the four fractions collected every 10 minutes. (**B-D**) MOLT-4 cells were treated with either vehicle, whole extract or fractions 1-4 (3 µg/mL) and (B) apoptosis was analyzed after 24 h (N=3) via Annexin V/PI, (C-D) NICD and cleaved caspase-3 (C. Cas. 3) expressions were evaluated (N=3) after 3 h with β-tubulin as the loading control. A representative blot is shown. (**E**) UHPLC/UV chromatogram of fraction 2, the specific compounds constituting the fraction are marked (C1-C5). (**F**) Chemical structure and peak assignment of CBD and 331-18A according to ^{1}H and ^{13}C NMR. Atom numbering is according to the monoterpene numbering system. (**G-I**) MOLT-4 cells were treated with the whole extract (3 µg/mL) or with 0.06 µg/mL 331-18A, 0.06 µg/mL CBDV and 1.5 µg/mL CBD, their corresponding concentrations in the extract, and their different combinations. Cells were assessed for (G) apoptosis after 24 h (N=3) via Annexin V/PI assay and (H-I) NICD expression after 3 h (N=3) with GAPDH as the loading control. Results are presents as mean ± SEM and statistically analyzed with One-way ANOVA (*$p<0.05$, **$p<0.01$, ***$p<0.001$).

123 **331-18A, CBDV and CBD mediate their effect through CB2 and TRPV1 to trigger Ca^{2+} flux**

124 Phytocannabinoids usually operate through specific cannabinoid receptors in the eCBS. To elucidate
125 which endocannabinoid receptors mediate the antitumor effect, we first evaluated in MOLT-4 cells the
126 mRNA expression of *CNR1* and *CNR2* (for CB1 and CB2, respectively), as well as G protein-coupled
127 receptor 55 (*GPR55)*, *TRPV1*, Transient receptor potential cation channel, subfamily A, member 1
128 (*TRPA1*) and Transient receptor potential cation channel subfamily M (melastatin) member 8 (*TRPM8*),
129 (**Fig. 2A**). The ΔCT results showed low expression for *CNR1*, *TRPA1* and *TRPM8*, medium expression
130 for *CNR2* and *GPR55*, and high expression for *TRPV1*. We tested antagonists for those receptors that had
131 either high or medium expression: TRPV1 (AMG9810), CB2 (AM630 or SR-144,528), GPR55 (CID),
132 and general Gq GPCR (BIM-46187) as a control, and evaluated whether they were able to rescue NICD
133 expression upon treatment with the whole extract (fig. S4A-B). Only the CB2 and TRPV1 antagonists
134 rescued the expression of NICD upon treatment with the whole extract, therefore we tested whether they
135 were able to rescue NICD expression after treatment with the combination of 331-18A, CBDV and CBD
136 (Fig. 2B-C). The CB2 antagonist rescued the expression from 56% to 87%, and the TRPV1 antagonist
137 rescued NICD expression to 100% by itself.

138 TRPV1 is a Ca^{2+} channel and eCBS receptors are known to trigger Ca^{2+} flux (*15*, *16*). Therefore, as the
139 next step we tested the effect of the three cannabinoids on cytosolic Ca^{2+} levels. We used the Fluo-4
140 calcium probe to measure the effect of 331-18A, CBDV and CBD combination on MOLT-4. Each of the
141 molecules separately caused some elevation in Ca^{2+}, but only their combination had an effect on Ca^{2+} to
142 the same extent as the whole extract (Fig. 2D). We tested Ca^{2+} levels when cells were pretreated with the
143 antagonists to CB2 and TRPV1. Both antagonists inhibited the elevation in response to the whole extract
144 (Supplementary fig. S3C, D). When 331-18A, CBDV and CBD were tested separately with antagonists
145 to either CB2 or TRPV1 (Fig. 2E), CB2 but not TRPV1 antagonist diminished 331-18A induced Ca^{2+}

146 increase, indicating this cannabinoid exerts its effect through CB2, while both antagonists significantly
147 decreased the Ca^{2+} elevation by CBDV and CBD. Next, we assessed whether inhibition of the receptors
148 rescues MOLT-4 cells from the cytotoxic properties of the cannabinoid combination (Fig. 2F). Treatment
149 with the inhibitors by themselves, separately or both together, did not induce MOLT-4 cell death. Upon
150 treatment with the combination of 331-18A, CBDV and CBD, inhibition of CB2 only partially rescued
151 the cells from treatment-induced apoptosis, reducing the apoptotic rate from 75% of the combination-

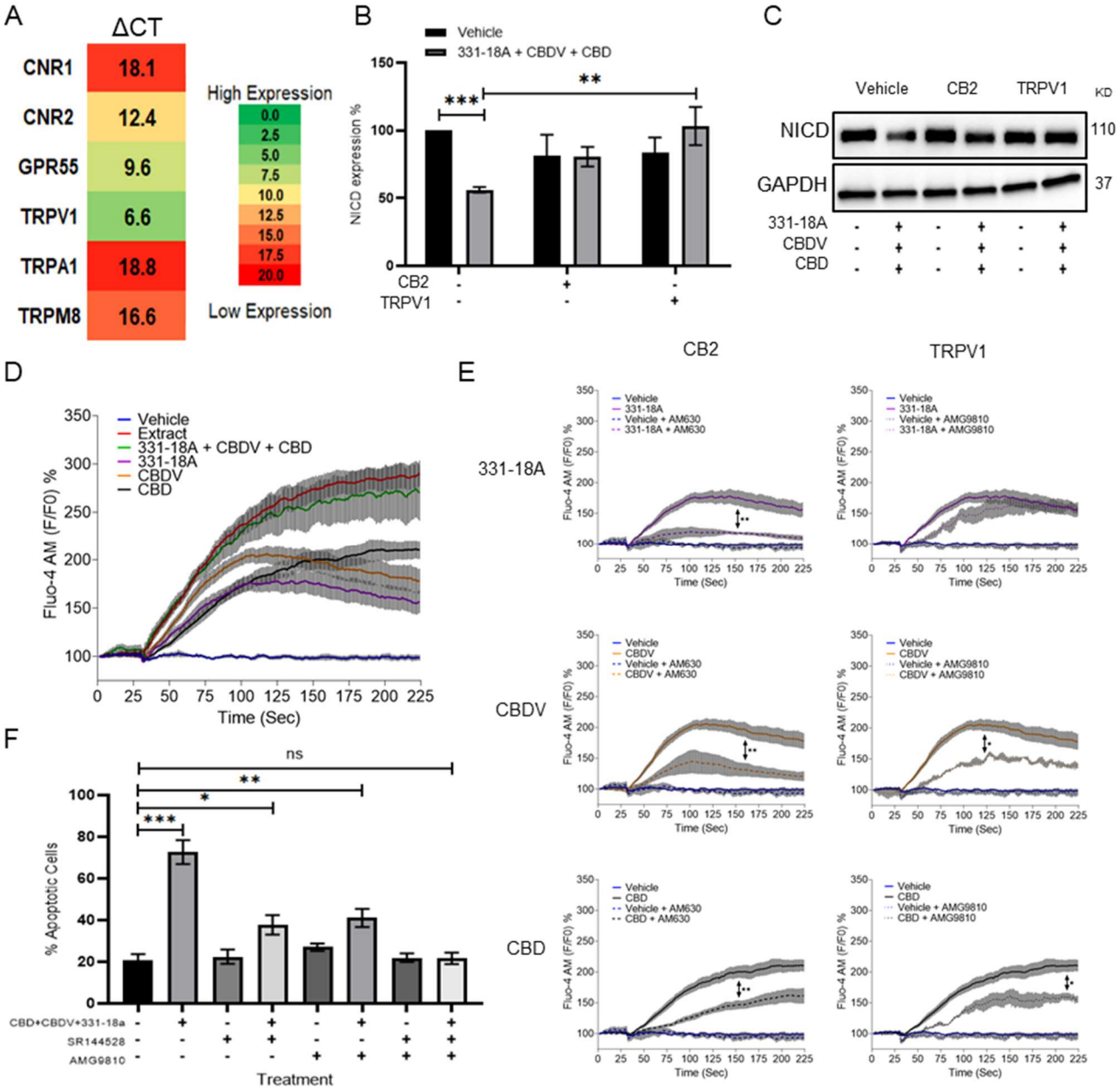

Fig. 2. 331-18A, CBDV and CBD mediate their effect through CB2 and TRPV1. (**A**) The mRNA levels of receptors *CNR1* (CB1), *CNR2* (CB2), *GPR55*, *TRPV1*, *TRPA1* and *TRPM8* were evaluated by qRT-PCR. Gene expression levels were calculated as ΔCT normalized to *GUSB* housekeeping gene. Results are presented as mean expression of three biological replicates. High ΔCT values indicate low receptor expression. (**B**) MOLT-4 cells were pretreated with 50 μM antagonist to CB2 (AM630) or TRPV1 (AMG9810) for 30 min, then treated with the combination of the three cannabinoids for 3 h. NICD expression was evaluated by western blot (N=3) with GAPDH as the loading control and statistically analyzed with an unpaired student's t-test (**p<0.01, ***p<0.001). (**C**) Representative blots of B. (**D**) Calcium release by MOLT-4 cells was measured with the Fluo-4 calcium probe immediately following treatment with either vehicle, whole extract, a combination of 331-18A, CBDV and CBD, and each cannabinoid separately. The calcium curves represent an average of three independent experiments. (**E**) Reduction of each phytocannabinoid-induced calcium release by pretreatment with 50 μM of antagonist to CB2 (AM630) or TRPV1 (AMG9810) for 30 min. The calcium curve for each compound is given again in this graph to compare the effects with the antagonists (N=3, two-way ANOVA, *p<0.05, **p<0.01). (**F**) MOLT-4 cells were pretreated with 50 μM antagonist to CB2 (SR-144,528) or TRPV1 (AMG9810) or both for 30 min, then treated with the combination of the three cannabinoids or left untreated. Apoptosis was analyzed after 24 h (N=3) by Annexin V/PI. Results are presented as mean ± SEM and statistically analyzed with one-way ANOVA (*p<0.05, **p<0.01, ***p<0.001).

152 treated cells to 40%. However, the apoptotic rate was still significantly higher than that of the untreated
153 control. Inhibition of TRPV1 only also partially rescued the cells, to ~50%, but again the apoptotic rate
154 remained significantly increased relative to the untreated control. Inhibition of both CB2 and TRPV1
155 simultaneously rescued the cells from treatment-induced apoptosis, confirming the effect of the three
156 cannabinoids is mediated through both receptors.

157 **Notch1 downregulation by cannabinoids is mediated through the integrated stress response**
158 **pathway**

159 To elucidate the mechanism by which the Notch1 pathway is down-regulated following treatment, we
160 used RNA-seq analysis to measure and compare the gene expression profile of MOLT-4 cells after 3 hours
161 of treatment with either vehicle or the whole extract (**Fig. 3A**). A list of the ten most increased- and
162 decreased-abundance genes following treatment is presented in supplementary table S4. ChaC
163 glutathione-specific γ-glutamylcyclotransferase 1 (*CHAC1*), a negative regulator of the Notch signaling
164 pathway (*34*), was identified as the second most increased-abundance gene. CHAC1 acts by inhibiting the
165 furin-like cleavage of Notch1, preventing the formation of the mature form of Notch1 (*35*), as we have

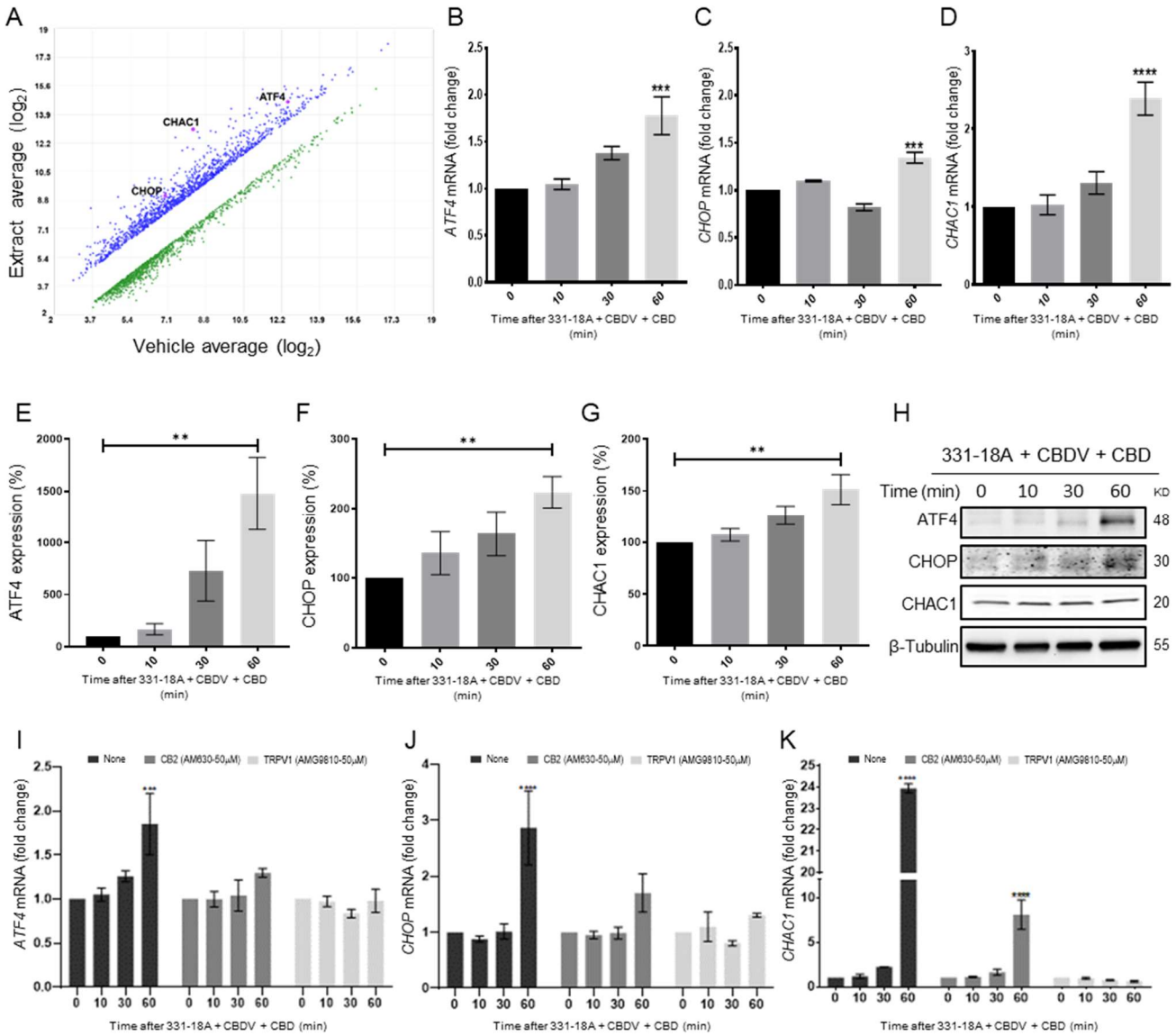

Fig. 3. Notch1 downregulation by 331-18A, CBDV and CBD combination is mediated via ATF4-CHOP-CHAC1 signaling pathway. (**A**) MOLT-4 cells were treated for 3 h with either vehicle or the whole Extract (3 µg/mL) and an RNA-seq (affymetrix) scatter plot presents the differential expression; the increased abundance genes *CHAC1*, *CHOP* and *ATF4* are marked (N=3). (**B-D**) MOLT-4 cells were treated for 3 h with 331-18A, CBDV and CBD combination (N=3), the mRNA expression of *ATF4*, *CHOP* and *CHAC1* genes was evaluated with qRT-PCR at different time points (0-60 min). Differences are presented as fold-change ± SEM and statistically analyzed with one-way ANOVA (***p<0.001, ****p<0.0001). (**E-G**) MOLT-4 cells were treated as in B-D and the protein expression of ATF4, CHOP and CHAC1 were evaluated with β-tubulin as the loading control. Intensity analysis was performed on three independent experiments (N=3) and statistically analyzed with an unpaired Student's *t*-test (**p<0.01). (**H**) Representative blots. (**I-K**) Analysis of ATF4, CHOP and CHAC1 mRNA expression at different time points following pretreatment with CB2 and TRPV1 antagonists for 30 min and then treatment with the cannabinoid combination (N=3), analyzed with two-way ANOVA (***p<0.001, ****p<0.0001).

166

167 previosly demonstrated upon treatment with the whole extract (*32*). C/EBP homologous protein (*CHOP*)
168 and Activating transcription factor 4 (*ATF4*), ER-stress signaling pathway markers that are upstream to
169 *CHAC1* (*36*), had also a significant increase in their abundance. We confirmed the RNA-seq results by
170 qRT-PCR showing that the mRNA of *ATF4*, *CHOP* and *CHAC1* is indeed significantly increased after
171 treatment with a combination of 331-18A, CBDV and CBD (Fig. 3B-D, respectively) or the whole extract
172 (fig. S3E-G). A significant increase was apparent 60 min after treatment. Using specific antibodies to
173 ATF4, CHOP and CHAC1, we verified the protein expression level of all three was also significantly
174 increased at 60 min after treatment (Fig. 3E-H). The protein expression levels of CHAC1 in MOLT-4 cells
175 were also significantly increased upon treatment with the whole extract (fig. S3H, I).
176 To further understand the mechanism, we evaluated how pretreatment with antagonists to the cannabinoid
177 receptors through which 331-18A, CBDV and CBD exert their effect, CB2 and TRPV1, affected *ATF4*,
178 *CHOP* and *CHAC1* expression following treatment (Fig. 3I-K). Inhibition of CB2 reduced the treatment-
179 induced increase in mRNA expression, but a trend of increase for ATF4 and CHOP remained at 60
180 minutes, and CHAC1 expression was significantly increased. Inhibition of TRPV1 rescued from
181 treatment-induced induction of all three targets. Similar effects were found when pretreatment with
182 antagonists to CB2 and TRPV1 was followed by treatment with the whole extract (fig. S3J-L); and the
183 increase in the expression levels of CHAC1 protein was abolished when MOLT-4 cells were treated by
184 either antagonist (fig. S3M). These results demonstrate that CB2 and TRPV1 participate in inducing
185 CHAC1 expression and preventing Notch1 maturation, resulting in a decrease in NICD release and cell
186 death.
187 We therefore speculated that the combination of the three cannabinoids caused the activation of ATF4-
188 CHOP-CHAC1 signaling by Ca^{2+} depletion and ER-stress (*37*). To further verify the role of ATF4-CHOP-
189 CHAC1 signaling in mediating the downregulation of the Notch1 pathway, we inhibited the activity of

the upstream target eukaryotic Initiation Factor-2α (eIF2α) in MOLT-4 cells using integrated stress response inhibitor (ISRIB), which inhibits the activity of eIF2α without affecting its phosphorylation (*38*) (fig. S5A-B). Then, we treated the cells with either vehicle or the combination of the cannabinoids. After 24 hours, blocking the activity of eIF2α prevented the cytotoxic effect of 331-18A, CBDV and CBD combination (**Fig. 4A**) or of the whole extract (fig. S5C). Moreover, eIF2α inhibition prevented the reduction in NICD expression upon treatment with either the whole extract (fig. S5D-E) or the cannabinoid combination (Fig. 4B-C). Inhibition of eIF2α also rescued the cells from the induced increase in the mRNA expression of ATF4, CHOP and CHAC1 upon treatment with the combination of the cannabinoids

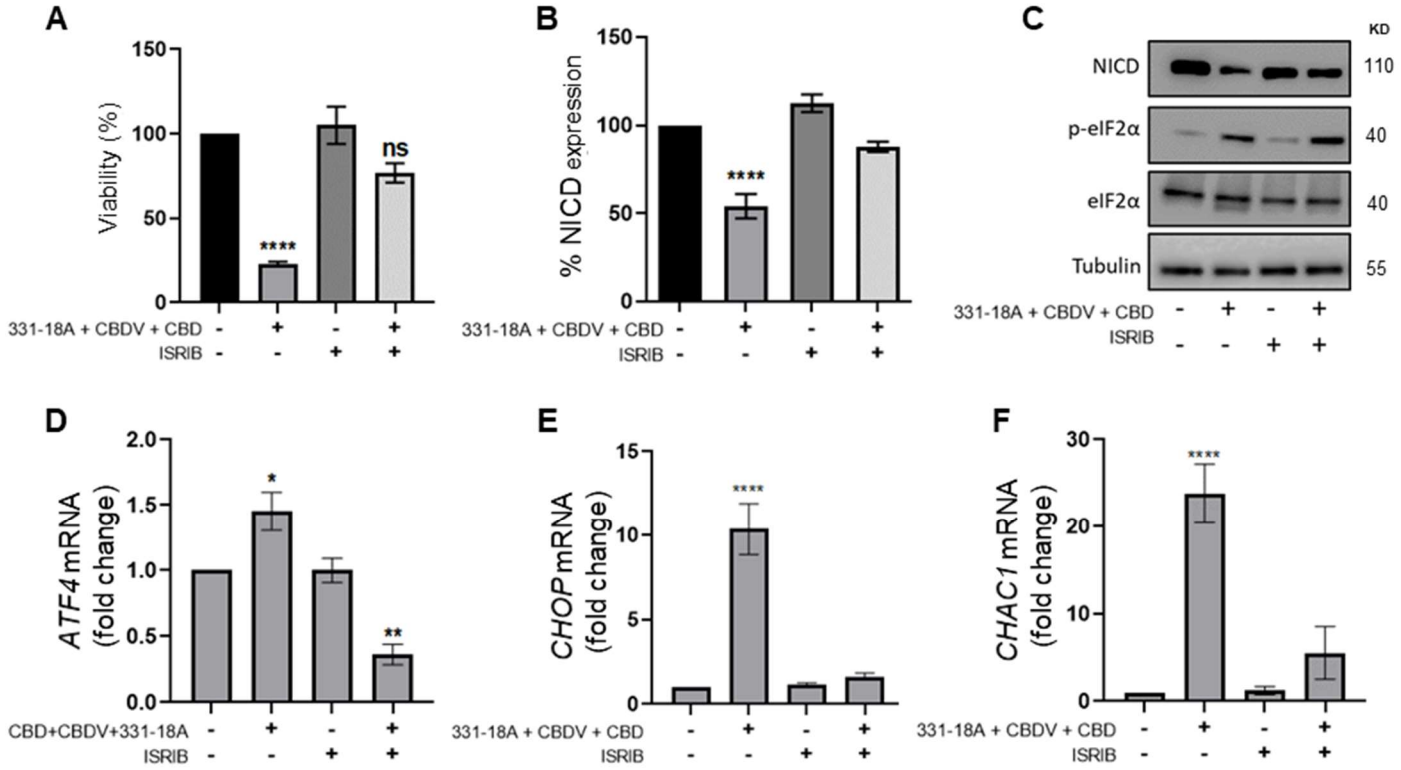

Fig. 4. 331-18A, CBDV and CBD combination activates eIF2α. MOLT-4 cells were pretreated for 30 min with the eIF2α inhibitor ISRIB (150 μM) or left untreated, then treated with vehicle or the combination of 331-18A, CBDV and CBD for 3 h. (**A**) Viability after 24 hrs was assessed with XTT (N=3). (**B**) NICD protein expression was assessed (N=3) with β-Tubulin as the loading control (unpaired Student's *t*-test, *p<0.05). (**C**) A representative image also showing the protein levels of phosphorylated eIF2α (Ser^{51}) and total eIF2α. (**D-F**) *ATF4*, *CHOP* and *CHAC1* gene expression was assessed via qRT-PCR 4 hrs after treatment (N=3). Results are presented as mean ± SEM and statistically analyzed with one-way ANOVA (****p<0.0001).

198 (Fig. 4D-F). Thus, inhibition of the integrated stress response pathway, eIF2α-ATF4-CHOP-CHAC1
199 signaling, rescued MOLT-4 cells from the cytotoxic effect of the combination of the three cannabinoids
200 and prevented the reduction in NICD expression, as well as the increased transcription of ATF4, CHOP
201 and CHAC1 upon treatment.

202 To further investigate the interaction between 331-18A,CBDV and CBD, we assessed their effect on the
203 viability of MOLT-4 cells in different relative proportions. First we tested the ability of each seaparate
204 cannabinoid to inhibit the proliferation of MOLT-4 cells in doses ranging 0-2 μg/ml (**Fig. 5A**), which is
205 below and above the overall concentration for which we found an effect for the cannabinoid combination.
206 331-18A and CBDV affected viability from a dose of 1 μg/ml and CBD from a dose of 0.5 μg/ml. Next,
207 we calculated the combination index of every pair and all three cannabinoids in concentrations ranging
208 from 0-2 μg/mL (Fig. 5B-E). The most synergistic area is displayed in red. We calculated the total synergy
209 score for the combination of all three cannabinoids relative to the pairwise combinations (Fig. 5F).
210 According to Highest Single Agent (HSA) reference model(*39*), a combination of CBDV with either 331-
211 18A or CBD results in a likely antagonistic interaction (score < -10), a combination of 331-18A and CBD
212 results in a likely additive interaction (score from -10 to 10), and only the combination of all three
213 cannabinoids is likely synergistic (score > 10, Fig. 5G).

214 **Inhibition of cancer progression in-vivo by 331-18A, CBDV and CBD combination**

215 We further evaluated the anti-tumor properties of the three cannabinoids using several mouse models. The
216 first model was a subcutaneous tumor model for which we have already demonstrated the effectivity of
217 the whole extract (*32*). We engrafted subcutaneously Nonobese diabetic-severe combined
218 immunodeficiency (NOD/Scid) mice with MOLT-4 cells, then treated with vehicle only or the
219 combination of the cannabinoids from when tumors reached a volume of 100 mm^3 (day 7), on alternating
220 days, for a duration of four weeks. Treatment with a combination of 331-18A, CBDV and CBD

221 significantly inhibited tumor growth (**Fig. 6A-C**). Significant differences were apparent approximately 3

222 weeks after treatment started (Fig. 6A), and at the endpoint, 34 days from the injection of cells, the average

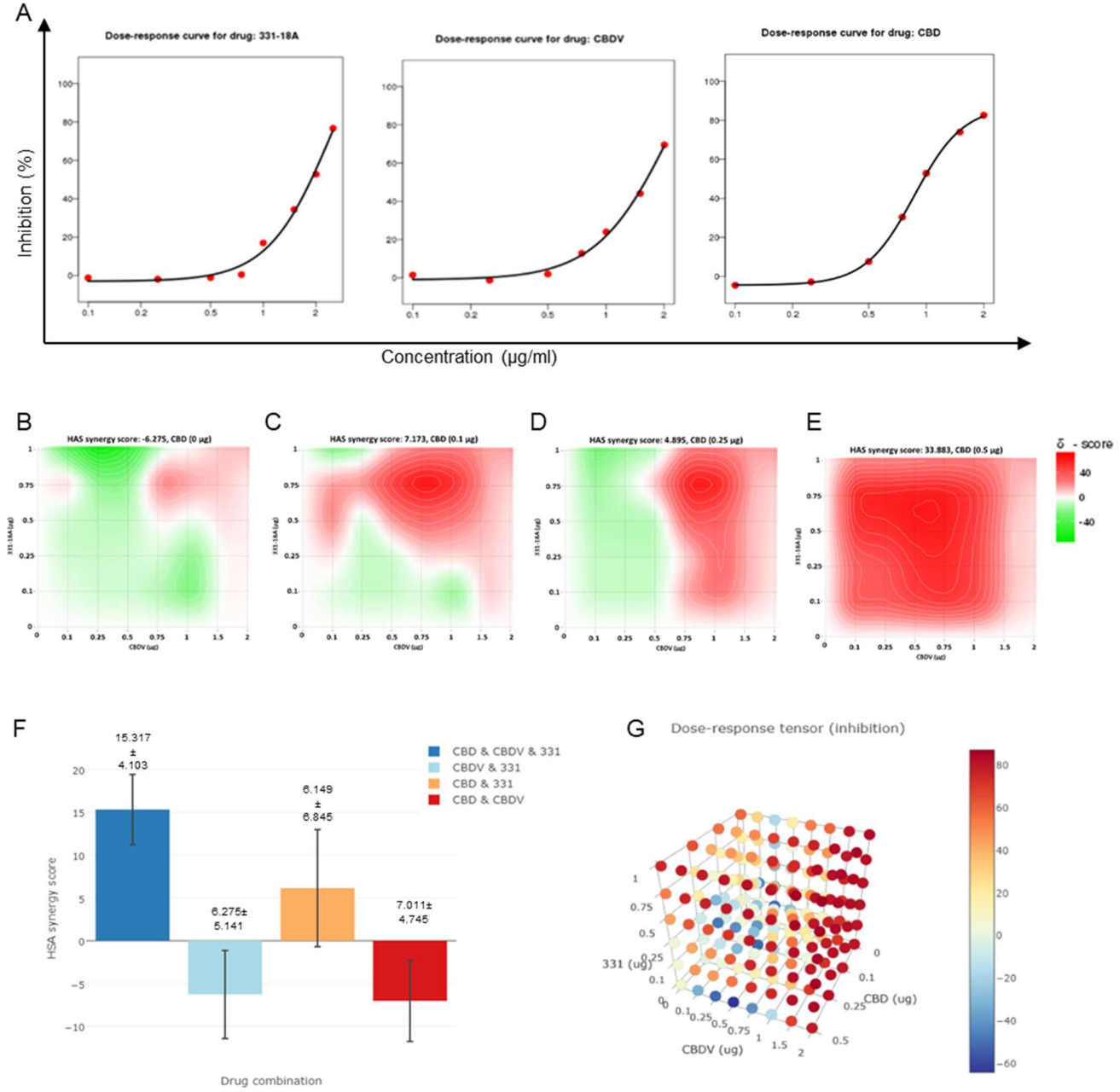

Fig. 5. All three cannabinoids must be combined for a synergistic effect. (**A**) MOLT-4 cell death (N=3) was assessed by XTT following treatments with concentrations ranging 0-2 µg/ml and a dose-response curve for each cannabinoid separatly was plotted. (**B-E**) Synergy distribution for different ratios of cannabinoids was calculated by HSA model with SynergyFinder web application (v 2.0), representative dose-response matrices are presented for CBD at (B) 0, (C) 0.1, (D) 0.25 and (E) 0.5 µg/ml. (**F-G**) Best synergy scores according to HSA model presented for the triple combination relative to the two-cannabinoid combinations.

weight of tumors was significantly lower in the treated group compared to the control group (Fig. 6B). Excised tumors (Fig. 6C) were analyzed for their cannabinoid content according to a method recently developed by our group for biological tissues (*40*). Using ESI-LC/MS, we identified and quantified each of the three cannabinoids in the tumors [16.0 ± 6.7, 22.3 ± 10.4 and 265.8 ± 109.7 ng/g for CBDV, 331-18A and CBD, respectively (average ± S.E.M., N=3)]. Notably, the ratio of the cannabinoids analyzed in the tumors was similar to the ratio given to the mice in the treatment protocol. In addition, a significant decrease was observed in NICD expression in the tumors treated with the cannabinoids (Fig. 6D). To assess possible toxicity, the body weight of the mice was monitored throughout the experiment (Fig. 6E). There were no significant differences in the average weight of mice in the control group and the treatment group.

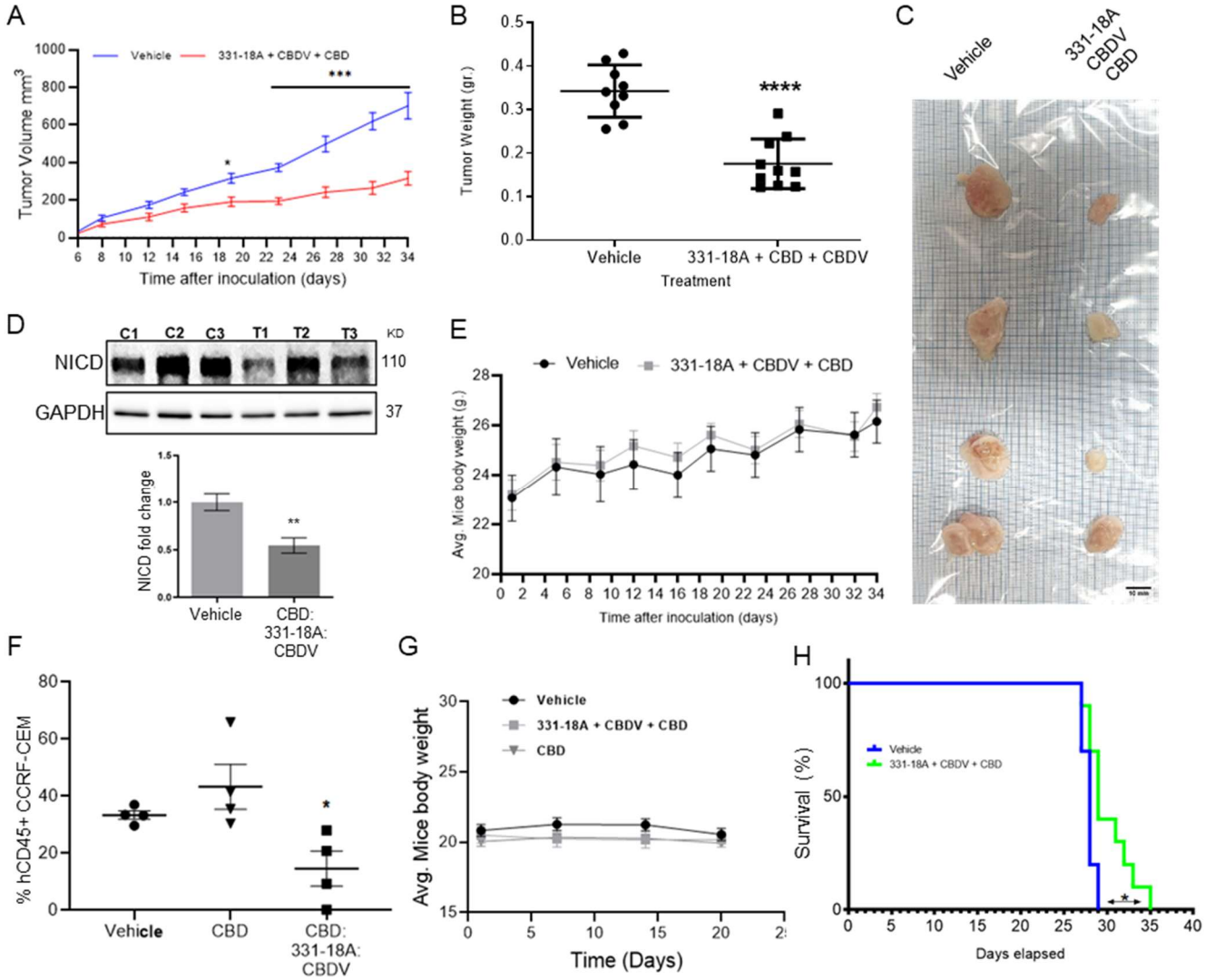

Fig. 6. Inhibition of cancer progression in-vivo by a combination of 331-18A, CBDV and CBD. (**A**) Female NOD/Scid mice (N=4-5/group, two independent experiments) were engrafted subcutaneously with 1×10^6 MOLT-4 cells. After seven days, the mice were randomly divided into two groups and alternate-day treated intraperitoneally with either vehicle or a combination of 331-18A (1.11 mg/kg), CBDV (1.11 mg/kg) and CBD (17.77 mg/kg). Ectopic tumor volume was measured using a vernier caliper and calculated according to the formula (length × width^2) × 0.5. The average difference between groups was statistically analyzed by Bonferroni's multiple comparisons test (*p<0.05, ***p<0.001). (**B**) After 34 days of treatment, the mice were sacrificed and tumors were excised and weighed (N=9). The difference in the weights of the tumors between treatment groups was statistically analyzed by unpaired Student's *t*-test (****p<0.0001). (**C**) Representative photograph of excised tumors. (**D**) A representative blot (*top*) and fold change (*bottom*) of NICD protein expression in excised tumors at day 34 after treatment with either vehicle (C) or a combination of the three cannabinoids (T), with GAPDH as the loading control. Data are presented as mean ± SEM (N=3) and statistically analyzed by unpaired Student's *t*-test (**p<0.01). (**E**) Body weight (grams) in vehicle- and cannabinoids-treated mice. (**F**) Female NSG mice were intravenously injected with 1×10^6 human CCRF-CEM cells. Mice were randomly divided into three groups (N=5/group) and treated intraperitoneally daily for five days, then left untreated for two days before starting another cycle, for a period of three weeks. Treatment groups were vehicle, pure CBD (30 mg/kg), and a combination of CBD (26.67 mg/kg), CBDV (1.67 mg/kg) and 331-18A (1.67 mg/kg) at the same overall concentration as pure CBD. After 24 days, the percentage of hCD45+ cells in the bone marrow was measured with flow cytometry and statistically analyzed by unpaired student's t-test (*p<0.05). (G) Body weight (grams) in vehicle- and cannabinoids-treated mice. (H) Survival analyses after CCRF-CEM injection followed by treatment with either vehicle or the cannabinoid combination (N=10/group), statistical differences were calculated with the Log-rank (Mantel-Cox) test (*p<0.05).

Next, we assessed the cannabinoids using an intravenous model which better resembles leukemogenesis (*41*, *42*). We engrafted NOD-SCID IL2rγ-null (NSG) mice that are a better host for human immune cells with CCRF-CEM, Notch1 mutated T-ALL cells. The mice were treated with a combination of the three cannabinoids, and to verify the need for the combination, one group was also treated with pure CBD in the same overall dose. At the endpoint of the experiment, the amount of human CD45+ cells detected in the bone marrow (BM) was significantly decreased in the mice treated with the combination of the three cannabinoids compared to the control, and compared to pure CBD (Fig. 6F). In this model as well, there were no significant differences in the average weight of the mice (Fig. 6G). The combination of 331-18A, CBDV and CBD was as effective as the whole extract (fig. S6A-B). In addition, the administration of the cannabinoid combination significantly prolonged survival in treated mice compared to the survival of vehicle-treated control mice (Fig. 6H), to a similar degree to the whole extract (fig. S6C).

244 **Discussion**

245 Targeting Notch signaling components has generated much interest for its therapeutic potential. However,
246 so far efforts to develop treatments that target Notch signaling have been unsuccessful (*43*). Cannabis, in
247 its many forms, is already being prescribed to cancer patients all over the world, mainly as a palliative
248 treatment for the inhibition of nausea and emesis associated with chemotherapy, appetite stimulation, pain
249 relief and relief from insomnia (*17*). On top of that, recent studies have demonstrated that
250 phytocannabinoids also possess anti-cancer potential (*24*, *25*, *31*, *44–46*).

251 In the current study, we identified three unique phytocannabinoids that together selectively induce
252 apoptosis in Notch1 mutated leukemia cells: CBD, CBDV and the novel phytocannabinoid 331-18A. CBD
253 and CBDV are well-known and commercially available. However, to the best of our knowledge, the third
254 phytocannabinoid 331-18A, denoted in the literature as 6,12-dihydro-6-hydroxy-cannabidiol (*47*), has not
255 been previously identified in natural and/or decarboxylated Cannabis plants. We suggest that the need for
256 all three cannabinoids for the optimal anti-tumor effect demonstrates the critical importance of elucidating
257 the individual and polypharmacological effects of the entire molecular spectrum of Cannabis.

258 Although CBD by itself demonstrated some capacity to induce cell death, it was only when all three
259 cannabinoids were combined that the same extent of response was achieved as treating with the whole
260 extract. The Cannabis plant produces a vast array of over 140 phytocannabinoids and hundreds of other
261 components, but the full extent of their biological effects and interactions is still not completely
262 understood. Nevertheless, mounting evidence suggests that their combined effect as a whole is greater
263 than that of each separate compound (*48*, *49*). Recently, Blasco-Benito *et al*. (*50*), have shown that a Δ^9-
264 THC-rich extract was much more potent than pure Δ^9-THC in producing antitumor responses in both cell
265 culture and animal models of breast cancer. However, they were unable to identify the combinations of
266 compounds that were responsible for this increased potency. In previous publications by our group, we
267 showed that different CBD-rich Cannabis extracts, with equal amounts of CBD but varying concentrations

268 of other minor compounds, lead to diverse anticonvulsant effects in a mouse model of epilepsy (*29*), and
269 selective antitumoral effects in Notch1-mutated in T-ALL (*32*); suggesting the potential therapeutic
270 effects of other compounds in the extracts in addition to CBD.

271 A possible mechanism previously suggested to explain the difference between the effects of purified
272 phytocannabinoids versus full-spectrum extracts is the "entourage effect", where one compound may
273 synergize the activity and efficacy of another on the same target (*48*, *49*). This "entourage effect" was
274 postulated by Russo (*48*) based on a phenomenon observed in the eCBS by Ben Shabbat *et al*. (*51*). While
275 it is well-established for endocannabinoids, only very few studies demonstrated this for
276 phytocannabinoids. We showed here that the presence of small amounts of the minor cannabinoids 331-
277 18A and CBDV enhanced the effect of CBD by itself. Our success in isolating and characterizing a
278 minimal number of cannabinoids that achieve the same antitumor effect as the whole extract is a
279 significant advancement in the field of medical Cannabis and provides solid evidence for the "entourage
280 effect".

281 Subsequent reports have expanded the notion of the "entourage effect" to polypharmaceutical and/or
282 polypharmacological effects, where several of the plant metabolites work simultaneously on the same
283 receptors, and/or when the same molecule has several different targets within the same system (*52–54*).
284 CBD has been shown to present complex signaling capabilities of many receptors in the extended eCBS.
285 Specifically, it was shown to have a weak affinity to CB2, and a strong affinity to many of the TRPV
286 family receptors, including TRPV1, TRPV2 and TRPV3 (*55*, *56*).

287 We suggest that the Notch1-mutated T-ALL cells are affected through the engagement of the eCBS
288 receptor CB2 and the channel TRPV1. More specifically, the known cannabinoids CBD and CBDV
289 affected both, while the novel 331-18A exerted its effect only through CB2. Following the stimulation of
290 the receptors, Ca^{2+} is depleted from the ER and there is an increase in cytosolic Ca^{2+} and activation of

291 eIF2α followed by ATF4-CHOP-CHAC1 signaling. Notably, the inhibition of eIF2α upstream to ATF4
292 rescued T-ALL cells from reduced NICD expression by treatment with 331-18A, CBDV and CBD
293 combination. The upregulation of CHAC1 inhibits the S1 furin-like cleavage of Notch1 at the Golgi
294 apparatus (*35*), leading to the arrival of immature Notch1 to the plasma membrane as we have previously
295 shown (*32*). This inhibition of the Notch1 pathway ultimately leads to apoptosis in T-ALL cells that rely
296 on mutated Notch1 for propagation (see schematic representation in Fig. 7).
297 The potential antitumor effects of cannabinoids through the Notch1 signaling pathway were previously
298 demonstrated in glioma, where THC induced the expression of p8 protein, upstream to ATF3/4 (*57*). These
299 findings suggest blocking Notch1 maturation through the eIF2α-ATF4-CHOP-CHAC1 pathway and
300 inhibiting the S1 furin-like cleavage of Notch1 have the potential to affect all types of activation mutations
301 in Notch1, and also all four human homologs of Notch (Notch1-4) (*35*, *58*). Our findings are potentially
302 relevant for numerous diseases, as dysregulation of Notch signaling has been found in various other
303 cancers including breast, prostate and colorectal; as well as in non-cancerous diseases (*8*, *9*, *12*). As such,
304 they may pave the way for the establishment of new pharmacotherapies for the treatment of Notch1-
305 dependent malignancies and other diseases.

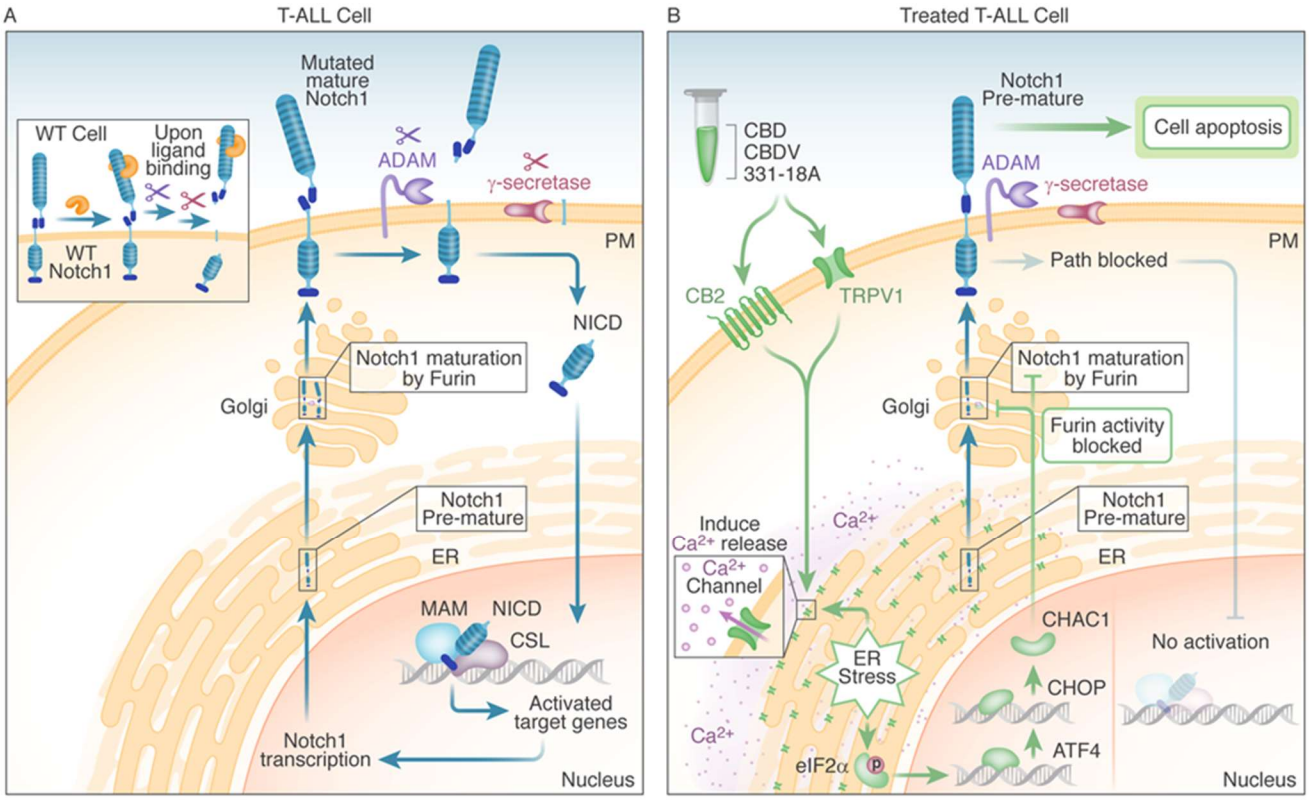

Fig. 7. Schematic representation. (**A**) In WT cells, the Notch1 receptor is only activated upon ligand binding. In T-ALL cells that have a Notch1 mutation, the receptor is constitutively active regardless of ligand binding, leading to a positive feedback loop in which the mature receptor is cleaved by a series of sequential cleavage events, causing the release of NICD, which translocates to the nucleus where it promotes transcription of target genes involved in cell growth. The premature Notch1 is cleaved by a furin-like convertase in the trans-Golgi apparatus, resulting in a mature receptor that is transported to the membrane. (**B**) The three phytocannabinoids CBD, CBDV and 331-18A in the whole extract stimulate CB2 and TRPV1 leading to an increase in cytosolic Ca^{2+} and ER stress induced activation of eIF2α followed by ATF4-CHOP-CHAC1 signaling. CHAC1 inhibits the furin-like cleavage of Notch1, preventing its maturation and resulting in reduced NICD formation, reduced cell viability and increased apoptosis.

318 **Materials and Methods**

319 **Reagents.** The analytical standards (>98%) for phytocannabinoids were purchased from Silicol Scientific
320 Equipment Ltd. (Or Yehuda, Israel). The antagonists CID 16020046 (#4959/5), AM630 (#1120/10), SR-
321 144,528 (#5039/10) and AMG9810 (#2316/10) were purchased from Tocris Bioscience (Bristol, UK).
322 BIM-46187 (#5332990001) and ISRIB (#SML0843) were purchased from Sigma-Aldrich (Rehovot,
323 Israel). Synthetic CBD, CBDV and 331-18A ware purchased from Cannasoul Analytics (Caesarea, Israel).
324 **Phytocannabinoids analysis.** Comprehensive phytocannabinoid analysis was performed using a UHPLC
325 system coupled to a Q Exactive™ Focus Hybrid Quadrupole-Orbitrap MS (Thermo Scientific, Bremen,
326 Germany) using a similar chromatographic method as previously described (*29*, *32*). MS acquisition was
327 carried out with a heated electro spray ionization (HESI-II) ion source operated in negative mode. Source
328 parameters were as follows: sheath gas flow rate, auxiliary gas flow rate and sweep gas flow rate: 50, 20
329 and 0 arbitrary units respectively; capillary temperature: 350°C; heater temperature: 50°C; spray voltage:
330 3.00 kV. The scan range was 150–550 m/z for all acquisition events. MS was operated in full MS^1 mode
331 at 70,000 resolution, and the AGC target was set to 10^6 with a maximum IT of 100 ms. Identification and
332 absolute quantification of phytocannabinoids was performed by external calibrations as described by
333 Berman *et al*.(*29*). Absolute quantification of phytocannabinoids with analytical standards was performed
334 by external calibrations. Standard mixes were prepared ranging from 1 to 1000 ng/mL for Δ^9-THCA, Δ^9-
335 THC, CBDA and CBD, and 0.25 to 625 ng/mL for all the other components. The dynamic range for each
336 component was determined as maximum deviation from expected concentrations of 20%, and minimum
337 signal-to-noise ratios of 10. All other phytocannabinoids without analytical standards were semi-
338 quantified according to calibration curves from the same phytocannabinoid family or average curves for
339 unknown compounds (*29*). All samples were injected and analyzed by ESI-LC/MS in three concentrations
340 (10, 1 and 0.1 µg/mL Cannabis extract to ethanol).

341 **Isolation of single phytocannabinoids.** Fractionation of the whole Cannabis extract into four fractions
342 and isolation of single phytocannabinoids were performed using a semi-preparative HPLC/UV (Thermo
343 Scientific, Bremen, Germany). The chromatographic separation was achieved using a Luna® C18 column
344 (10 µm, 250 mm × 21.1 mm i.d.) and a two-solvent A/B multistep gradient (solvent A: 0.1% acetic acid
345 in water and solvent B: 0.1% acetic acid in acetonitrile, the solvents and acetic acid were of HPLC and
346 LC/MS grades, respectively). The multistep gradient program was established as follows: initial
347 conditions were 50% B for 4 min, raised to 76% B until 6.5 min, held at 76% B for 16.5 min, and then
348 raised to 90% B until 26 min, held at 90% B until 31 min, decreased to 50% B over the next 4 min, and
349 held at 50% B until 40 min for re-equilibration of the system prior to the next injection. A flow rate of 20
350 ml/min and an injection volume of 500-750 µl were used. Data acquisition was performed at 220 nm. The
351 crude Cannabis extract was prepared in a concentration of 100 mg/ml in ethanol. Fractions were collected
352 in 10 min intervals and then lyophilized to dryness and analyzed by UHPLC/UV and ESI-LC/MS.
353 To improve the yield and purity of the fractions for isolation of single phytocannabinoids, a preliminary
354 separation step was employed prior to semi-preparative HPLC fractionation. The crude Cannabis extract
355 was dissolved to a concentration of 0.5 g/ml in ethanol, filtered using a PTFE 0.45 µm filter, and then
356 purified using a PLC 2050 Purification System, equipped with a CPC-250 column and a photodiode array
357 (PDA) detector (Gilson Inc.). Separations were achieved using a biphasic solvent system consisting of
358 upper (hexane:acetonitrile in the ratio of 98:2 v/v) and mobile (acetonitrile:water in the ratio 50:50 v/v)
359 phases in descending mode. The column was operated with a flow rate of 12.5 ml/min and a rotation speed
360 of 2,200 rpm. The gradient program was established as follows: initial conditions were
361 acetonitrile:water:hexane in the ratio 50:50:0 v/v for 25 min, and then gradually raised to
362 acetonitrile:water:hexane in the ratio 64:34:2 v/v until 45 min. All the solvents were of HPLC grade. The

363 collected fractions were lyophilized to dryness and then subjected to semi-preparative HPLC fractionation.
364 The specific phytocannabinoids were collected according to retention time.

365 **Structure elucidation.** The structure of the isolated 331-18A was elucidated by ^{1}H and ^{13}C one-
366 dimensional NMR spectra (Avance-III-700, Bruker, Germany) with CBD as the reference. The samples
367 were dissolved in $CDCl_3$ and analyzed at 4ºC with Tetramethylsilane as the internal reference. The optical
368 rotation of 331-18A in comparison to CBD was determined in chloroform (10 mg/mL) using a Jasco P-
369 1010 (Rudolph Research Analytical, US) polarimeter at 26ºC.

370 **Cell culture.** The T-cell leukemia cell lines MOLT-4 (CVCL_0013, CRL-1582™) and CCRF-CEM
371 (CVCL_0207, CCL-119™) were purchased from ATCC. Cell lines were grown in RPMI 1640 media
372 (Sigma-Aldrich; R8758), and kept at 37ºC in a 5% carbon dioxide incubator. Unless otherwise stated, all
373 culture media were supplemented with 10% FBS (Biological Industries; 04-007-1A), penicillin (100
374 U/mL) and streptomycin (100 µg/mL) (Biological Industries; 03-031-1B).

375 **Cell apoptosis assay.** Cells were cultured in 12-well plates at 1×10^{6} cells/well with media containing
376 0.5% FBS and incubated for 24 h with either DMSO (vehicle), Cannabis extract 12, fractions 1-4 and
377 different combinations of 0.06 µg/ml 331-18A, 0.06 µg/ml CBDV and 1.5 µg/ml CBD. Apoptotic cells
378 were detected by an Annexin V/PI assay using flow cytometry or by detection of cleaved caspase-3.

379 **Annexin V/PI assay.** Apoptosis was assessed by Annexin V-FITC (BioVision; 1006-200, 1:500) and PI
380 staining in an annexin binding buffer (BioVision; 1006-100; 1:500) according to the manufacturer's
381 instructions. Apoptosis assessed by flow cytometry used a BD™ LSR II digital four-laser flow cytometer
382 (BD Biosciences) and was analyzed by BD FACSDiva™ software version 6.1.2. (BD Biosciences).
383 Results were calculated as percentage of positive Annexin V-FITC cells out of total cells counted (30,000
384 events).

385 **Western blot analysis.** Cells were quickly washed twice with ice-cold PBS, and lysed in
386 radioimmunoprecipitation assay buffer (RIPA) lysis buffer (Sigma Aldrich; R0278) freshly supplemented
387 with protease and phosphate inhibitors (Cell Signaling Technology; 5872). Lysates were cleared by
388 centrifugation at 13,000 g at 4ºC for 10 min. Protein concentration was determined by a Bradford assay
389 (Sigma Aldrich; B6916). Proteins were denatured in NuPAGE™ LDS Sample Buffer (4X) (Thermo
390 Fisher; NP0008) and supplemented with β-mercaptoethanol (Sigma Aldrich; B6131). Typically, 20-50
391 mg of total protein were loaded per lane on a Novex™ 4-20% Tris-Glycine gradient gel (Invitrogen;
392 XP04202BOX) and electrophoretically transferred to a nitrocellulose membrane (Bio-Rad; 1704159S).
393 Membranes were blocked with TBS 0.1% Tween 20 buffer containing 5% bovine serum albumin (Sigma;
394 A7906) for 1 h and incubated with the primary antibody overnight at 4°C. This was followed by incubation
395 with horseradish peroxidase-labeled matching secondary antibodies. Immunoreactive bands were detected
396 by Luminata™ HRP substrate (Millipore; WBLUR0500) and visualized using a MicroChemi imager
397 (DNR Bioimaging Systems). Antibodies used: Cleaved Notch1 Val1744 (CST, 4147S; AB_2153348;
398 1:1,000) to assess NICD, cleaved caspase-3 (CST, 9664; AB_2070042; 1:1,000), β-tubulin (CST; clone
399 D3U1W, 86298; AB_2715541; 1:1,000), GAPDH (CST, 2118; AB_561053; 1:5,000), ATF4
400 (Proteintech, 10835-1-AP; AB_2058600; 1:500), CHOP (Proteintech, 15204-1-AP; AB_2292610; 1:500),
401 CHAC1 (abcam, ab76386; AB_1658635; 1:500), eIF2α (CST, 5324; AB_10692650; 1:1000) and
402 Phospho-eIF2α (Ser51) (CST, 3398; AB_2096481; 1:1000). Secondary antibodies include: Peroxidase
403 AffiniPure Goat Anti-Rabbit IgG (H+L) (Jackson ImmunoResearch, 111-035-144; AB_2307391;
404 1:5,000) and Peroxidase-AffiniPure Goat anti mouse IgG (HZ+L) (Jackson ImmunoResearch, 115-035-
405 003; AB_10015289; 1:5000).
406 **RNA extraction.** Total RNA was isolated from MOLT-4 cells (1×10^6 cells/sample) using TRIzol®
407 (Thermo Fisher; 15596026) and RNeasy kit (Qiagen; 74104) according to the manufacturer's instructions.

408 Sample quality was assessed both spectrophotometrically (Nanodrop Technologies®) and by gel
409 electrophoresis with 1% agarose.

410 **RNA-seq.** RNA sequencing of differentially expressed genes was performed on extracted RNA with an
411 Affymetrix Clariom-S microarray for human genome RNA expression analysis and an Affymetrix
412 Transcriptome Analysis Console software. The threshold set for increased- and decreased-abundance
413 genes was a fold change ≥1.5 and $p<0.05$. The sequencing was performed by the Center
414 for Genomic Technologies of The Hebrew University of Jerusalem.

415 **Quantitative RT-PCR.** cDNA was synthesized from 1 µg of extracted RNA. Purified RNA was reverse
416 transcribed with the qScript™ cDNA synthesis kit (Quanta Biosciences; 95047). The mRNA expression
417 levels of were quantified using qRT-PCR 7300 system (Applied Biosystems) using Human Taqman
418 probes (Thermo Fisher Scientific) for: *GAPDH* (Hs02758991_g1); *CNR1* (CB1) (Hs01038522_s1); *CNR2*
419 (CB2) (Hs00361490_m1); *GPR55* (Hs00271662_s1); *TRPV1* (Hs00175798_m1); *TRPM8*
420 (Hs01066596_m1); *TRPA1* (Hs00175798_m1); *ATF4* (Hs00909569_g1); *DDIT3* (CHOP)
421 (Hs00358796_g1); *CHAC1* (Hs00225520_m1). Relative expression values were normalized using to the
422 endogenous housekeeping gene *GAPDH* as the control and calculated using standard ΔCT methods.

423 **Calcium imaging.** MOLT-4 Cells were loaded with the fluorescein Ca^{2+} probe Fluo-4 AM (Invitrogen #
424 F14217). Cells were incubated for 60 min in RPMI medium and supplemented with 1 µM Fluo-4/AM.
425 Cells were then rinsed twice and incubated for another 30 min in a Fluo-4 AM-free HBSS buffer (Sigma
426 Aldrich #H6648). During these steps the cells were kept in the dark. Fluo-4 signals were collected by a
427 BD™ LSR II digital four-laser flow cytometer (BD Biosciences) and analyzed by BD FACSDiva™
428 software version 6.1.2. (BD Biosciences).

429 **Cell viability assay.** Cells were cultured in 96-well plates. At 1×10^5 cells/well the media was replaced
430 with RPMI containing 0.5% FBS and treatments as indicated. DMSO was used as the vehicle. The XTT-

431 based cell proliferation kit (Sartorius, Beit Haemek, Israel) was used to quantitate viability according to
432 the manufacturer's instructions. Cytotoxicity was measured following 24 hrs of incubation using
433 fluorescence spectrophotometry at excitation and emission wavelengths of 450-500 and 630-690 nm,
434 respectively, and calculated as percent reduction between treated and control cells.

435 **Synergy Scoring**. The cell viability percentage for each concentration was assessed with an XTT-based
436 cell proliferation kit (Sartorius, Beit Haemek, Israel), then entered into SynergyFinder web application (v
437 2.0). The HSA model was used to calculate synergy scores of the cannabinoid combinations. Estimation
438 of outlier measurements was carried out with cNMF algorithm (*59*) implemented in SynergyFinder.

439 **Mice and procedures.** All procedures were performed according to protocols approved by the Technion
440 Administrative Panel of Laboratory Animal Care (animal protocol number: IL_0470317). Female
441 NOD.CB17-Prkdcscid/NCrHsd (IMSR_ENV:HSD-170) adult (6-7 weeks) mice were purchased from
442 Envigo. Female NSG adult (6-7 weeks) mice were purchased from the Technion animal facility.

443 For the in-vivo tumorigenicity assay, MOLT-4 cells mixed with BD Matrigel^{TM} Matrix Growth Factor
444 Reduced (BD; FAL356230) (1:1 v/v) were injected subcutaneously into the flanks of 7-week-old female
445 NOD-scid mice. Tumor size was measured with a caliper, and the tumor volume was determined
446 according to the formula: length x width^2 x 0.5. The mice were euthanized after the indicated days as none
447 reached the maximal endpoint size (1 cm^3). The xenograft tumors were dissected and weighed.

448 For the in-vivo leukemogenesis assay and survival analysis, CCRF-CEM cells were intravenously injected
449 to 7-week female NSG mice. The bone marrow was harvested from each mouse and the infiltrated CCRF
450 cells were identified by staining for a human CD45 antibody (Biolegend; AB_2687375; BLG-368522;
451 1:200).

452 **Cannabinoids analysis from tumor tissue.** Fresh excised tumors were accurately weighed and dissected
453 to smaller sections. Hanks' Balanced Salt Solution (Sigma Aldrich; H8264) was added in a ratio of 1 ml

454 per 100 mg sample. The samples were further homogenized into single-cell suspensions with a
455 gentleMACS™ Dissociator (Miltenyi Biotec) using a pre-set program for tumor tissues. The single cell
456 suspensions were stored at -80ºC until further extraction. CBD, CBDV and 331-18A were analyzed using
457 the ESI-LC/MS system by retention time, accurate mass and spectral matching against our developed ESI-
458 LC/MS/MS library of phytocannabinoids (*29*). Absolute quantification of the three compounds was
459 performed by the stable isotope dilution method as recently described by our group (*40*). Briefly, the
460 extraction solution (methanol:acetonitrile:acetic acid in the ratio 50:50:0.1 v/v) spiked with 20 ng/mL of
461 CBD-d3 internal standard (Sigma-Aldrich; C-084) was added to the single cell suspensions in the ratio
462 3:1 v/v, respectively. Samples were thoroughly vortexed and then centrifuged for 20 min at 4ºC for protein
463 and cell precipitation. The supernatants were then mixed in a ratio of 1:3 v/v sample to 0.1% v/v acetic
464 acid in water, and loaded onto Agela Cleanert C8 solid phase extraction cartridges (500 mg of sorbent, 50
465 µm particle size). Cannabinoids were eluted from the columns using 2 ml of 0.1% v/v acetic acid in
466 methanol, evaporated to dryness by speedvac, and reconstituted in 100 µl ethanol. Since there was no
467 analytical standard available for 331-18A, this compound was semi-quantified according to the calibration
468 curve of CBD.

469 **Statistics and reproducibility**. Data were analyzed with GraphPad Prism software version 7.04.
470 Statistical significance was determined by either an unpaired two-tailed Student's *t*-test (with unequal
471 variations if an F test ruled out the equal variation assumption) or one-way ANOVA followed by Sidak's
472 multiple comparisons test for multiple groups. Kaplan–Meier survival curves were analyzed with the
473 Gehan–Breslow–Wilcoxon test, as appropriate for the dataset. Data are generally expressed as mean ±
474 SEM, as denoted in the Figure captions, with $p \leq 0.05$ was considered statistically significant.

475 **Supplementary Materials**
476
477 **Table S1**. Phytocannabinoid concentrations by UHPLC/LC-MS of fractions relative to the whole
478 extract.
479
480 **Table S2**. Phytocannabinoid concentrations by UHPLC/LC-MS of cannabis fraction 2 peaks.
481
482 **Table S3**. ^{1}H and ^{13}C peak assignments and chemical shifts of 331-18A.
483
484 **Table S4.** Ten most increased- and decreased-abundance genes following treatment of MOLT-4 cells
485 with the whole extract according to RNA sequencing.
486
487 **Fig. S1**. Fraction 2 is as effective as the whole extract in reducing the viability of MOLT-4 cells.
488
489 **Fig. S2**. Specific identification of phytocannabinoids with anti-cancer properties by spectral matching
490 and peak purity.
491
492 **Fig. S3**. CBD and 331-18A NMR spectra.
493
494 **Fig. S4**. Notch1 downregulation by Extract 12 is mediated through CB2 and TRPV1 followed by ATF4-
495 CHOP-CHAC1 signaling pathway.
496
497 **Fig. S5**. Whole extract treatment activates eIF2α.
498
499 **Fig. S6**. Inhibition of tumor growth *in-vivo* by whole extract.

500 **References**
501

502 1. T. Girardi, C. Vicente, J. Cools, K. De Keersmaecker, The genetics and molecular biology of T-
503 ALL. **129**, 1113–1123 (2017).
504 2. E. Vadillo, E. Dorantes-Acosta, R. Pelayo, M. Schnoor, T cell acute lymphoblastic leukemia (T-
505 ALL): New insights into the cellular origins and infiltration mechanisms common and unique
506 among hematologic malignancies. *Blood Rev.* **32**, 36–51 (2018).
507 3. C. Sorrentino, A. Cuneo, G. Roti, Therapeutic Targeting of Notch Signaling Pathway in
508 Hematological Malignancies. *Mediterr. J. Hematol. Infect. Dis.* **11**, e2019037 (2019).
509 4. A. A. Ferrando, The role of NOTCH1 signaling in T-ALL. *Hematol. Am. Soc. Hematol. Educ.*
510 *Progr.*, 353–361 (2009).
511 5. A. C. McCarter, Q. Wang, M. Chiang, Notch in Leukemia. *Adv. Exp. Med. Biol.* **1066**, 355–394
512 (2018).
513 6. Z. Fang-Fang, Y. You, L. Wen-Jun, Progress in research on childhood T-cell acute lymphocytic
514 leukemia, Notch1 signaling pathway, and its inhibitors: A review. *Bosn. J. Basic Med. Sci.*
515 (2020), doi:10.17305/bjbms.2020.4687.
516 7. M. Katoh, M. Katoh, Precision medicine for human cancers with Notch signaling dysregulation
517 (Review). *Int. J. Mol. Med.* **45** (2020), pp. 279–297.
518 8. H. Qiu, P. M. Zmina, A. Y. Huang, D. Askew, B. Bedogni, Inhibiting Notch1 enhances
519 immunotherapy efficacy in melanoma by preventing Notch1 dependent immune suppressive
520 properties. *Cancer Lett.* **434**, 144–151 (2018).
521 9. M. A. Rice, E. C. Hsu, M. Aslan, A. Ghoochani, A. Su, T. Stoyanova, Loss of Notch1 activity
522 inhibits prostate cancer growth and metastasis and sensitizes prostate cancer cells to antiandrogen
523 therapies. *Mol. Cancer Ther.* **18**, 1230–1242 (2019).
524 10. J. Li, Q. Li, L. Lin, R. Wang, L. Chen, W. Du, C. Jiang, R. Li, Targeting the Notch1 oncogene by
525 miR-139-5p inhibits glioma metastasis and epithelial-mesenchymal transition (EMT). *BMC*
526 *Neurol.* **18**, 133 (2018).
527 11. S. A. Kahn, X. Wang, R. T. Nitta, S. Gholamin, J. Theruvath, G. Hutter, T. D. Azad, L. Wadi, S.
528 Bolin, V. Ramaswamy, R. Esparza, K.-W. Liu, M. Edwards, F. J. Swartling, D. Sahoo, G. Li, R.
529 J. Wechsler-Reya, J. Reimand, Y.-J. Cho, M. D. Taylor, I. L. Weissman, S. S. Mitra, S. H.
530 Cheshier, Notch1 regulates the initiation of metastasis and self-renewal of Group 3
531 medulloblastoma. *Nat. Commun.* **9**, 4121 (2018).
532 12. K. E. Vinson, D. C. George, A. W. Fender, F. E. Bertrand, G. Sigounas, The Notch pathway in
533 colorectal cancer. *Int. J. Cancer*. **138**, 1835–1842 (2016).
534 13. F. Punzo, I. Manzo, C. Tortora, E. Pota, V. D'Angelo, G. Bellini, A. Di Paola, F. Verace, F.
535 Casale, F. Rossi, Effects of CB2 and TRPV1 receptors' stimulation in pediatric acute T-
536 lymphoblastic leukemia. *Oncotarget*. **9**, 21244–21258 (2018).
537 14. K.-H. Jeon, S.-H. Park, W. J. Bae, S. W. Kim, H. J. Park, S. Kim, T. H. Kim, S. H. Jeon, I. Park,
538 H.-J. Park, Y. Kwon, Cannabidiol, a Regulator of Intracellular Calcium and Calpain. *Cannabis*
539 *cannabinoid Res.* (2022), doi:10.1089/CAN.2021.0197.
540 15. C. Muller, P. Morales, P. H. Reggio, E. Murillo-Rodriguez, C. Chiu, J. Hee Hong, Cannabinoid
541 Ligands Targeting TRP Channels (2019), doi:10.3389/fnmol.2018.00487.
542 16. A. Laguerre, K. Keutler, S. Hauke, C. Schultz, Regulation of Calcium Oscillations in β-Cells by
543 Co-activated Cannabinoid Receptors. *Cell Chem. Biol.* **28**, 88-96.e3 (2021).
544 17. D. I. Abrams, M. Guzman, Cannabis in cancer care. *Clin. Pharmacol. Ther.* **97**, 575–586 (2015).
545 18. D. I. Abrams, Using Medical Cannabis in an Oncology Practice. *Oncology*. **30**, 397–404 (2016).

19. M. Duran, E. Pérez, S. Abanades, X. Vidal, C. Saura, M. Majem, E. Arriola, M. Rabanal, A. Pastor, M. Farré, N. Rams, J.-R. R. Laporte, D. Capellà, Preliminary efficacy and safety of an oromucosal standardized cannabis extract in chemotherapy-induced nausea and vomiting. *Br. J. Clin. Pharmacol.* **70**, 656–663 (2010).
20. C. Pagano, G. Navarra, L. Coppola, M. Bifulco, C. Laezza, Molecular Mechanism of Cannabinoids in Cancer Progression. *Int. J. Mol. Sci.* **22**, 3680 (2021).
21. O. Kovalchuk, I. Kovalchuk, Cannabinoids as anticancer therapeutic agents. *Cell Cycle*. **19**, 961–989 (2020).
22. E. M. O'Reilly, J. M. Cosgrave, W. M. Gallagher, A. S. Perry, Plant-derived cannabinoids as anticancer agents. *Trends in cancer*. **8**, 350–357 (2022).
23. C. Blázquez, L. González-Feria, L. Álvarez, A. Haro, M. L. Casanova, M. Guzmán, Cannabinoids inhibit the vascular endothelial growth factor pathway in gliomas. *Cancer Res.* **64**, 5617–5623 (2004).
24. S. D. McAllister, L. Soroceanu, P.-Y. Y. Desprez, The Antitumor Activity of Plant-Derived Non-Psychoactive Cannabinoids. *J. Neuroimmune Pharmacol.* **10**, 255–267 (2015).
25. B. Hinz, R. Ramer, Cannabinoids as anticancer drugs: current status of preclinical research. *Br. J. Cancer 2022 1271*. **127**, 1–13 (2022).
26. K. M. Kampa-Schittenhelm, O. Salitzky, F. Akmut, B. Illing, L. Kanz, H. R. Salih, M. M. Schittenhelm, Dronabinol has preferential antileukemic activity in acute lymphoblastic and myeloid leukemia with lymphoid differentiation patterns. *BMC Cancer*. **16**, 25 (2016).
27. K. A. Scott, A. G. Dalgleish, W. M. Liu, Anticancer effects of phytocannabinoids used with chemotherapy in leukaemia cells can be improved by altering the sequence of their administration. *Int. J. Oncol.* **51**, 369–377 (2017).
28. M. Olivas-Aguirre, L. Torres-López, J. S. Valle-Reyes, A. Hernández-Cruz, I. Pottosin, O. Dobrovinskaya, Cannabidiol directly targets mitochondria and disturbs calcium homeostasis in acute lymphoblastic leukemia. *Cell Death Dis.* **10**, 779 (2019).
29. P. Berman, K. Futoran, G. M. Lewitus, D. Mukha, M. Benami, T. Shlomi, D. Meiri, A new ESI-LC/MS approach for comprehensive metabolic profiling of phytocannabinoids in Cannabis. *Sci. Rep.* **8**, 14280 (2018).
30. L. O. Hanuš, S. M. Meyer, E. Muñoz, O. Taglialatela-Scafati, G. Appendino, Phytocannabinoids: a unified critical inventory. *Nat. Prod. Rep.* **33**, 1357–1392 (2016).
31. L. Baram, E. Peled, P. Berman, B. Yellin, E. Besser, M. Benami, I. Louria-Hayon, G. M. Lewitus, D. Meiri, The heterogeneity and complexity of *Cannabis* extracts as antitumor agents. *Oncotarget*. **10**, 4091–4106 (2019).
32. E. Besser, A. Gelfand, G. M. Lewitus, H. Novak-Kotzer, S. Procaccia, P. Berman, I. Louria-Hayon, I. Shreiber-Livne, Y. Ofran, D. Meiri, Antitumoral effects of cannabis in Notch1-mutated T-cell acute lymphoblastic leukemia. *Cancer Commun.* **43**, 711–715 (2023).
33. L. Marchetti, V. Brighenti, M. C. Rossi, J. Sperlea, F. Pellati, D. Bertelli, Use of 13C-qNMR Spectroscopy for the Analysis of Non-Psychoactive Cannabinoids in Fibre-Type Cannabis sativa L. (Hemp). *Molecules*. **24** (2019), doi:10.3390/molecules24061138.
34. P.-H. Chen, W.-L. Shen, C.-M. Shih, K.-H. Ho, C.-H. Cheng, C.-W. Lin, C.-C. Lee, A.-J. Liu, K.-C. Chen, The CHAC1-inhibited Notch3 pathway is involved in temozolomide-induced glioma cytotoxicity. *Neuropharmacology*. **116**, 300–314 (2017).
35. Z. Chi, J. Zhang, A. Tokunaga, M. M. Harraz, S. T. Byrne, A. Dolinko, J. Xu, S. Blackshaw, N. Gaiano, T. M. Dawson, V. L. Dawson, Botch promotes neurogenesis by antagonizing Notch. *Dev. Cell*. **22**, 707–20 (2012).

592 36. J. H. Joo, E. Ueda, C. D. Bortner, X. P. Yang, G. Liao, A. M. Jetten, Farnesol activates the
593 intrinsic pathway of apoptosis and the ATF4-ATF3-CHOP cascade of ER stress in human T
594 lymphoblastic leukemia Molt4 cells. *Biochem. Pharmacol.* **97**, 256–268 (2015).
595 37. K. Zhai, A. Liskova, P. Kubatka, D. Büsselberg, Calcium entry through trpv1: A potential target
596 for the regulation of proliferation and apoptosis in cancerous and healthy cells. *Int. J. Mol. Sci.*
597 **21**, 1–25 (2020).
598 38. M. Halliday, G. R. Mallucci, Review: Modulating the unfolded protein response to prevent
599 neurodegeneration and enhance memory. *Neuropathol. Appl. Neurobiol.* **41**, 414–427 (2015).
600 39. B. Yadav, K. Wennerberg, T. Aittokallio, J. Tang, Searching for Drug Synergy in Complex
601 Dose–Response Landscapes Using an Interaction Potency Model. *Comput. Struct. Biotechnol. J.*
602 **13**, 504–513 (2015).
603 40. P. Berman, L. Sulimani, A. Gelfand, K. Amsalem, G. M. Lewitus, D. Meiri, Cannabinoidomics –
604 An analytical approach to understand the effect of medical Cannabis treatment on the
605 endocannabinoid metabolome. *Talanta*, 121336 (2020).
606 41. M. W. Lee, H. J. Kim, K. H. Yoo, D. S. Kim, J. M. Yang, H. R. Kim, Y. H. Noh, H. Baek, H.
607 Kwon, M. H. Son, S. H. Lee, H. W. Cheuh, H. L. Jung, K. W. Sung, H. H. Koo, Establishment of
608 a bioluminescent imaging-based in vivo leukemia model by intra-bone marrow injection. *Int. J.*
609 *Oncol.* **41**, 2047–2056 (2012).
610 42. Q. Xin, Z. Chen, W. Wei, Y. Wu, Animal models of acute lymphoblastic leukemia:
611 Recapitulating the human disease to evaluate drug efficacy and discover therapeutic targets.
612 *Biochem. Pharmacol.* **198**, 114970 (2022).
613 43. R. A. Previs, R. L. Coleman, A. L. Harris, A. K. Sood, Molecular pathways: Translational and
614 therapeutic implications of the notch signaling pathway in cancer. *Clin. Cancer Res.* **21**, 955–961
615 (2015).
616 44. E. B. Russo, J. Marcu, Cannabis Pharmacology: The Usual Suspects and a Few Promising Leads.
617 *Adv. Pharmacol.* **80**, 67–134 (2017).
618 45. G. Velasco, C. Sánchez, M. Guzmán, Anticancer mechanisms of cannabinoids. *Curr. Oncol.* **23**,
619 S23-32 (2016).
620 46. M. Guzmán, Cannabinoids: Potential anticancer agents. *Nat. Rev. Cancer*. **3**, 745–755 (2003).
621 47. P. Stoss, P. Merrath, A Useful Approach Towards Δ9 -Tetrahydrocannabinol. *Synlett*. **1991**, 553–
622 554 (1991).
623 48. E. B. Russo, Taming THC: Potential cannabis synergy and phytocannabinoid-terpenoid entourage
624 effects. *Br. J. Pharmacol.* **163**, 1344–1364 (2011).
625 49. T. Worth, Cannabis's chemical synergies. *Nature*. **572**, S12–S13 (2019).
626 50. S. Blasco-Benito, M. Seijo-Vila, M. Caro-Villalobos, I. Tundidor, C. Andradas, E. García-
627 Taboada, J. Wade, S. Smith, M. Guzmán, E. Pérez-Gómez, M. Gordon, C. Sánchez, Appraising
628 the "entourage effect": Antitumor action of a pure cannabinoid versus a botanical drug
629 preparation in preclinical models of breast cancer. *Biochem. Pharmacol.* **157**, 285–293 (2018).
630 51. S. Ben-Shabat, E. Fride, T. Sheskin, T. Tamiri, M.-H. H. Rhee, Z. Vogel, T. Bisogno, L. De
631 Petrocellis, V. Di Marzo, R. Mechoulam, An entourage effect: inactive endogenous fatty acid
632 glycerol esters enhance 2-arachidonoyl-glycerol cannabinoid activity. *Eur. J. Pharmacol.* **353**,
633 23–31 (1998).
634 52. R. Mechoulam, S. Ben-Shabat, From gan-zi-gun-nu to anandamide and 2-arachidonoylglycerol:
635 The ongoing story of cannabis. *Nat. Prod. Rep.* **16**, 131–143 (1999).
636 53. E. B. Russo, The Case for the Entourage Effect and Conventional Breeding of Clinical Cannabis:
637 No "Strain", No Gain. *Front. Plant Sci.* **9**, 1969 (2018).

638 54. V. Di Marzo, F. Piscitelli, The Endocannabinoid System and its Modulation by
639 Phytocannabinoids. *Neurotherapeutics*. **12**, 692–698 (2015).
640 55. B. Kis, F. C. Ifrim, V. Buda, S. Avram, I. Z. Pavel, D. Antal, V. Paunescu, C. A. Dehelean, F.
641 Ardelean, Z. Diaconeasa, C. Soica, C. Danciu, Cannabidiol—from Plant to Human Body: A
642 Promising Bioactive Molecule with Multi-Target Effects in Cancer. *Int. J. Mol. Sci.* **20**, 5905
643 (2019).
644 56. L. de Petrocellis, P. Orlando, A. S. Moriello, G. Aviello, C. Stott, A. A. Izzo, V. di Marzo,
645 Cannabinoid actions at TRPV channels: effects on TRPV3 and TRPV4 and their potential
646 relevance to gastrointestinal inflammation. *Acta Physiol.* **204**, 255–266 (2012).
647 57. A. Carracedo, M. Lorente, A. Egia, C. Blázquez, S. García, V. Giroux, C. Malicet, R. Villuendas,
648 M. Gironella, L. González-Feria, M. A. Piris, J. L. Iovanna, M. Guzmán, G. Velasco, The stress-
649 regulated protein p8 mediates cannabinoid-induced apoptosis of tumor cells. *Cancer Cell*. **9**, 301–
650 12 (2006).
651 58. I. N. Mungrue, J. Pagnon, O. Kohannim, P. S. Gargalovic, A. J. Lusis, CHAC1/MGC4504 Is a
652 Novel Proapoptotic Component of the Unfolded Protein Response, Downstream of the ATF4-
653 ATF3-CHOP Cascade. *J. Immunol.* **182**, 466–476 (2009).
654 59. A. Ianevski, A. K. Giri, P. Gautam, A. Kononov, S. Potdar, J. Saarela, K. Wennerberg, T.
655 Aittokallio, Prediction of drug combination effects with a minimal set of experiments. *Nat. Mach.*
656 *Intell.* **1**, 568–577 (2019).
657
658

Acknowledgments

We thank the the Israel Cancer Research Fund, Evelyn Gruss Lipper Charitable Foundation and the Israeli Ministry of Agriculture and Rural Development for their financial support of this work. The authors would like to thank Cannasoul Analytics and especially Dr. Rotem Perry Feigenbaum and Yogev Nir for the isolation of the phytocannabinoid compounds; Dr. Hugo Gottlieb and Dr. Michal Afri from the NMR unit at Bar Ilan University for performing the NMR measurements and deciphering the structure of the 331-18A phytocannabinoid; Moshe Barkaly for the semi-preparative HPLC fractionations of the whole extract; and Dr. Dafna Antes for the graphic scheme illustration. The authors declare no competing financial interests.

Funding:

Israel Cancer Research Fund grant 21-112-PG (DM)
Gruss Lipper Charitable Foundation grant 2027093 (DM)
Israeli Ministry of Agriculture and Rural Development 14370001 (DM)

Author contributions:

Conceptualization: E.B., S.P. and D.M.
Methodology: E.B. and P.B.
Investigation: E.B., A.G. and P.B.
Analysis and interpretation of data: E.B., A.G., P.B and S.P.
Writing-original draft: E.B. and D.M.
Writing-review & editing: E.B., D.M., P.B. and S.P.
Study supervision: D.M.

Competing interests

A patent pertaining to the results of the paper has been applied for the use of cannabinoids in the treatment of Notch-related diseases. This patent was licensed to Cavnox Ltd. to test the combination of the molecules in human clinical trials.

Data and materials availability

The RNA-Seq data that support the findings of this study have been deposited in the Gene Expression Omnibus under the accession code GSE154287.
https://www.ncbi.nlm.nih.gov/geo/query/acc.cgi?acc=GSE154287.
All data generated or analyzed during this study are included in this published article and its supplementary information files.